Available online at www.sciencedirect.com
ScienceDirect
Advances in Space Research 51 (2013) 209–218
ADVANCES IN SPACE RESEARCH (a COSPAR publication)
www.elsevier.com/locate/asr

The PAMELA space experiment

W. Menn [a,*], O. Adriani [b,c], G.C. Barbarino [d,e], G.A. Bazilevskaya [f], R. Bellotti [g,h], M. Boezio [i], E.A. Bogomolov [j], L. Bonechi [b,c], M. Bongi [c], V. Bonvicini [i], S. Borisov [l,k,m], S. Bottai [c], A. Bruno [g,h], F. Cafagna [h], D. Campana [e], R. Carbone [e,l], P. Carlson [n], M. Casolino [l], G. Castellini [o], L. Consiglio [e], M.P. De Pascale [l,k], C. De Santis [k], N. De Simone [l,k], V. Di Felice [k], A.M. Galper [m], W. Gillard [n], L. Grishantseva [m], G. Jerse [p,i], A.V. Karelin [m], S.V. Koldashov [m], S.Y. Krutkov [j], A.N. Kvashnin [f], A. Leonov [m], V. Malakhov [m], V. Malvezzi [k], L. Marcelli [k], A.G. Mayorov [m], V.V. Mikhailov [m], E. Mocchiutti [i], A. Monaco [g,h], N. Mori [b,c], N. Nikonov [j,l,k], G. Osteria [e], F. Palma [l,k], P. Papini [c], M. Pearce [n], P. Picozza [l,k], C. Pizzolotto [i], M. Ricci [q], S.B. Ricciarini [c], R. Sarkar [i], L. Rossetto [n], M. Simon [a], R. Sparvoli [l,k], P. Spillantini [b,c], S.J. Stochaj [r], J.C. Stockton [r], Y.I. Stozhkov [f], A. Vacchi [i], E. Vannuccini [c], G. Vasilyev [j], S.A. Voronov [m], J. Wu [n], Y.T. Yurkin [m], G. Zampa [i], N. Zampa [i], V.G. Zverev [m]

[a] *Universität Siegen, FB Physik, Walter-Flex-Str. 3, 57068 Siegen, Germany*
[b] *University of Florence, Department of Physics, I-50019 Sesto Fiorentino, Florence, Italy*
[c] *INFN, Sezione di Florence, I-50019 Sesto Fiorentino, Florence, Italy*
[d] *University of Naples "Federico II", Department of Physics, I-80126 Naples, Italy*
[e] *INFN, Sezione di Naples, I-80126 Naples, Italy*
[f] *Lebedev Physical Institute, RU-119991, Moscow, Russia*
[g] *University of Bari, Department of Physics, I-70126 Bari, Italy*
[h] *INFN, Sezione di Bari, I-70126 Bari, Italy*
[i] *INFN, Sezione di Trieste, I-34149 Trieste, Italy*
[j] *Ioffe Physical Technical Institute, RU-194021 St. Petersburg, Russia*
[k] *INFN, Sezione di Rome "Tor Vergata", I-00133 Rome, Italy*
[l] *University of Rome "Tor Vergata", Department of Physics, I-00133 Rome, Italy*
[m] *Moscow Engineering and Physics Institute, RU-11540 Moscow, Russia*
[n] *KTH, Department of Physics, and the Oskar Klein Centre for Cosmoparticle Physics, AlbaNova University Centre, SE-10691 Stockholm, Sweden*
[o] *IFAC, I-50019 Sesto Fiorentino, Florence, Italy*
[p] *University of Trieste, Department of Physics, I-34147 Trieste, Italy*
[q] *INFN, Laboratori Nazionali di Frascati, Via Enrico Fermi 40, I-00044 Frascati, Italy*
[r] *New Mexico State University, Las Cruces, NM 88003, USA*

Available online 6 July 2011

Abstract

On the 15th of June 2006, the PAMELA satellite-borne experiment was launched from the Baikonur cosmodrome and it has been collecting data since July 2006. The apparatus is comprised of a time-of-flight system, a silicon-microstrip magnetic spectrometer, a silicon-tungsten electromagnetic calorimeter, an anticoincidence system, a shower tail counter scintillator and a neutron detector. The combination of these devices allows precision studies of the charged cosmic radiation to be conducted over a wide energy range (100 MeV to 100's GeV) with high statistics. The primary scientific goal is the measurement of the antiproton and positron energy spectra in order to

* Corresponding author.
E-mail address: menn@pamela.physik.uni-siegen.de (W. Menn).

0273-1177/$36.00
doi:10.1016/j.asr.2011.06.030

search for exotic sources, such as dark matter particle annihilations. PAMELA is also searching for primordial antinuclei (anti-helium), and testing cosmic-ray propagation models through precise measurements of the antiparticle energy spectrum and precision studies of light nuclei and their isotopes. Moreover, PAMELA is investigating phenomena connected with solar and earth physics. After 4 years of operation in flight, PAMELA is now delivering coherent results about spectra and chemical composition of the charged cosmic radiation, allowing scenarios of production and propagation of cosmic rays to be fully established and understood.

Keywords: Cosmic rays; Antimatter; Satellite-borne experiment

1. Introduction

When Victor Hess discovered cosmic rays one hundred years ago, an impressive experimental study began. Now we know that cosmic rays are a sample of solar, galactic and extragalactic matter which includes the nuclei of all elements and their isotopes known in the periodic table, as well as electrons, positrons, and antiprotons. They are associated with the most energetic events and active objects in the Universe: supernovae explosion, pulsars, relativistic jets, active galactic nuclei.

The chemical composition and energy spectrum of cosmic rays give extensive information about their origin, acceleration and propagation mechanisms. The energies of the observed particles cover more than 13 magnitudes (from 10 s of MeV to above 10^{20} eV) and far exceed those reached by the most powerful accelerators. The energy spectra have been explored by direct methods (balloon-borne and satellite experiments) up to 10^{14} eV and by indirect methods (ground-based large-size apparatuses) up to 10^{20} eV at the highest energies.

At medium energies the study of antimatter and antiparticle content in cosmic rays is a unique tool to investigate several physics and astrophysical phenomena. The search for antimatter is strictly connected with the baryon antibaryon asymmetry in the Universe. Therefore, detection of antimatter of primary origin in cosmic rays would be a discovery of fundamental significance. If there was primordial antimatter, antihelium would be the most likely form to be detected in cosmic rays, likewise in matter primordial nucleosynthesis in which helium is the next most abundant element to hydrogen. The present observational limit in the search for antihelium is of the order of 10^{-7} in the antihelium-to-helium ratio. The PAMELA instrument will search for antihelium in an unprecented large energy range from a few hundred MeV to 600 GeV with a level of better than 10^{-6}.

Antiprotons and positrons are not direct indicators for the existence of antimatter domains, because they are primarily produced by collisions of the cosmic rays with the ISM. By measuring cosmic antiprotons and positrons one can probe astrophysics scenarios and unconventional particle physics. For example, local astrophysical sources such as nearby and young pulsars would appear as a distortion of the detected secondary production fluxes of electrons and positrons.

Another distortion of the secondary spectrum might come from dark matter annihilation or other exotic sources. There is strong evidence from several observations that the Universe is predominently composed of dark matter and dark energy. Among the most plausible candidates for dark matter are weakly interacting massive particles (WIMP), with the supersymmetric neutralino as a favourite candidate. Other models of WIMPs privilege lightest Kaluza–Klein particles in the Universal Extra Dimension scenario.

The PAMELA instrument is capable of measuring antiprotons and positrons with unprecedented statistics in an energy regime not explored so far.

Since the possible contributions from dark matter annihilation or other exotic sources are mixed with a huge background produced in the interactions of cosmic rays with the ISM, a detailed knowledge of the standard mechanisms of production, acceleration and transport of cosmic rays is required.

Parallel to the measurement of antimatter PAMELA is performing accurate measurements of the electron, proton and light nuclei energy spectra over a wide dynamic range.

In this sample cosmic-ray electrons are a small but important component of the cosmic radiation. Precision measurements of the electron component provide important information about the origin and propagation of cosmic rays in the Galaxy. Due to their low mass and the intergalactic magnetic field, cosmic-ray electrons undergo severe energy losses during their propagation in the Galaxy. Therefore they provide information regarding the origin and propagation of cosmic rays in the Galaxy that is not accessible from the study of the cosmic-ray nuclear components due to their differing energy-loss processes.

On the other hand, the determination of the proton and helium absolute fluxes will give information about the early Universe, whereas the nuclei composition and energy spectra measurements will allow us to learn about the origin and evolution of the matter content of our Galaxy; both spectra are related to fundamental physical processes that govern the dynamics of the Universe. The secondary/primary ratios of cosmic ray nuclear and isotopic abundances such as B/C, Be/C, Li/C and ^{3}He/^{4}He are studied with high statistics.

2. The PAMELA instrument

The PAMELA experiment is performed by an international collaboration of scientists from Italy, Russia, Germany and Sweden.

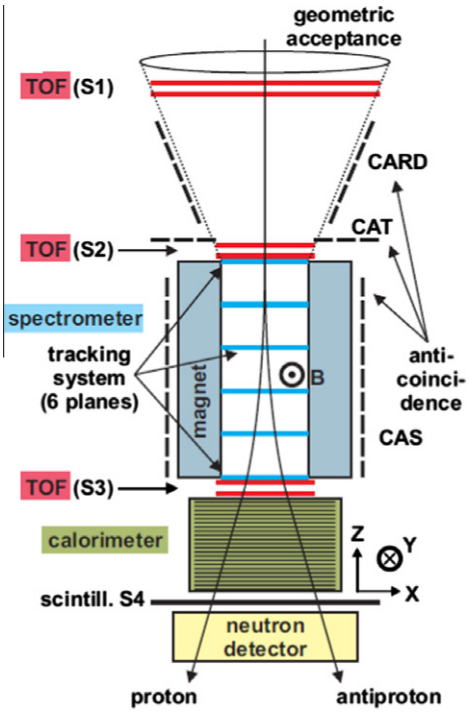

Fig. 1. A sketch of the PAMELA telescope. The method of discrimination between particle and antiparticle with the magnetic spectrometer is illustrated. The main direction of the magnetic field B inside the spectrometer is also shown.

The PAMELA apparatus, shown in Fig. 1, is composed of several sub-detectors: TOF system, anticoincidence system (CARD, CAS, CAT), magnetic spectrometer with microstrip silicon tracking system, W/Si electromagnetic imaging calorimeter, shower-tail-catcher scintillator (S4) and neutron detector.

A detailed description of the PAMELA instrument and an overview of the mission can be found in Picozza et al. (2007). The instrument has a maximum diameter of 102 cm and height of 120 cm; its mass is 470 kg, the maximum power consumption is 355 W. The core of the instrument is a magnetic spectrometer, made of a permanent magnet (0.43 T) and a silicon tracking system (resolution in the bending side 4 μm) for a maximum detectable rigidity of 1 TV. The dimensions of the permanent magnet define the geometrical factor of the PAMELA experiment to be 21.5 cm^2 sr. The magnetic spectrometer determines the charge sign and momentum of the incoming particle through the trajectory reconstruction in the magnetic field. A time-of-flight system consisting of three double layers (S1, S2, S3) of segmented plastic scintillator provides timing and dE/dx measurements and defines the primary PAMELA trigger; it will also identify downward-going particles.

The separation between hadronic and leptonic components at lower energies is provided by the velocity measurement (obtained from the trajectory and time-of-flight) and by an imaging W/Si detector and a neutron counter for kinetic energies above 1 GeV. The silicon calorimeter and the neutron detector assure a rejection of protons, compared to positrons, of the order of 10^5. The calorimeter permits also measurements of the electron energy up to 300 GeV, with a resolution of a few per cent.

More technical details can be found in Picozza et al. (2007). PAMELA has been inserted in a pressurized vessel and installed on board the Russian satellite DK-1 dedicated to Earth observation. It was launched on June 15th 2006 by a Soyuz-U rocket from the Baikonur cosmodrome in Kazakhstan in an elliptical orbit, ranging between 350 and 610 km and with an inclination of 70°. Since July 2006 PAMELA is delivering daily 16 GB of data to the Ground Segment in Moscow.

3. Data analysis and results

3.1. Analysis

The results presented here correspond to the data-set collected between July 2006 and December 2008. More than 10^9 triggers were accumulated during a total acquisition time of approximately 500 days.

3.2. Measurement of antimatter

The main scientific goal of PAMELA is the measurement of antimatter in the cosmic rays. It is not an easy task to identify the rare antimatter out of the vast background of the normal matter. The main background in the antimatter sample comes from like-charged particles (electrons in the antiproton sample and protons in the positron sample). This background is related to the capability of the instrument to perform electron–hadron separation.

At high energies there is an additional source from "spillover" (protons in the antiproton sample and electrons in the positron sample). This spillover background comes from the wrong determination of the charge sign due to the intrinsic deflection uncertainty in spectrometer measurements at the highest energies. This effect sets a limit to the maximum rigidity up to which the measurement can be extended.

3.3. Antimatter (antiprotons)

For kinetic energies above 1 GeV PAMELA combines the rigidity measurement of the spectrometer and the properties of the energy deposit and interaction topology in the calorimeter to identify the particles. Due to the longitudinal and transverse segmentation of the calorimeter, combined with dE/dx measurements from the individual silicon strips, electromagnetic showers can be identified with very high accuracy. The resulting electron contamination was estimated to be negligible across the whole energy range of interest.

An additional contamination of the selected proton and antiproton samples is due to pions, which are produced locally by cosmic-ray interactions with the PAMELA payload. This contamination was studied using both simulated

and flight data: at rigidities below 1 GV it is possible to identify negatively and positively-charged pions in the flight data using the velocity measurement of the TOF system once the calorimeter rejected electrons and positrons from the sample.

For the simulation we impinged protons isotropically on PAMELA from above and from the side, using the experimental proton spectrum measured by PAMELA as input. For the pion production both GHEISHA and FLUKA generators (Hofverberg, 2008; Bruno, 2008) were considered. We found that it was possible to reject most of the pions by applying strict selection criteria on the scintillators of the anticoincidence system and on the energy deposits in either S1 or S2. By comparing the results from flight data with the simulation, we estimated the residual pion contamination over the entire energy range, resulting in less than 5% contamination above 2 GV, decreasing to less than 1% above 5 GV.

To eliminate the proton background from spillover, a set of strict selection criteria (number of hits used for the fit, cut on the χ^2 value, etc.) was imposed on the quality of the fitted tracks. Additionally for each track the maximum detectable rigidity (MDR) was evaluated on an event-by-event basis by propagating the estimated coordinate errors and taking into account the track topology. The MDR had to be 6 times larger than the measured rigidity.

In this way the antiproton measurement could be extended up to 180 GV/c with acceptable contamination from spillover protons. We estimated the contamination using the GPAMELA detector simulation which is based on the GEANT3 package (Brun et al., 1994), see Bruno (2008) for details.

Finally we could derive the absolute antiproton spectrum and the antiproton-to-proton flux ratio from 60 MeV to 180 GeV, which is the largest energy range achieved so far.

Fig. 2 shows the antiproton energy spectrum and Fig. 3 shows the antiproton-to-proton flux ratio measured by PAMELA along with other recent experimental data and theoretical calculations assuming pure secondary production of antiprotons during the propagation of cosmic rays in the Galaxy (Adriani et al., 2010b).

The PAMELA data are in excellent agreement with recent data from other experiments. The antiproton flux shows the expected peak around 2 GeV (due to the kinematic constraints on the antiproton production) and is in overall agreement with pure secondary calculations. The antiproton-to-proton flux ratio increases smoothly with energy up to about 10 GeV and then levels off.

So in both cases the data follow the trend expected from secondary production calculations. The experimental uncertainties are smaller than the spread in the different theoretical curves and, therefore, provide important constraints on parameters relevant for secondary production calculations and contributions from exotic sources, e.g. dark matter particle annihilations.

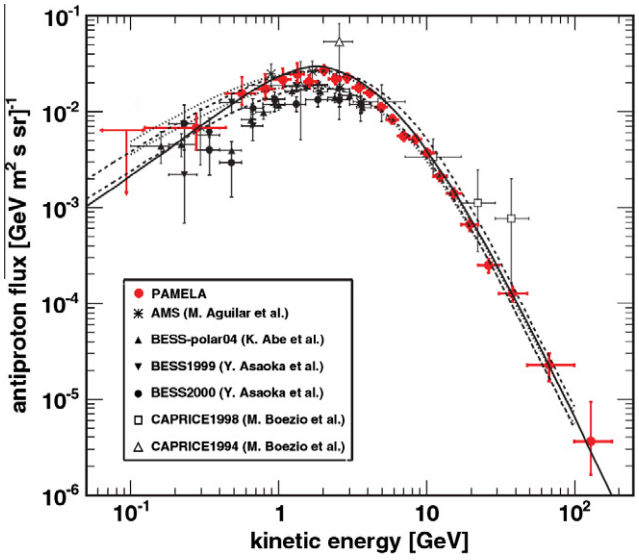

Fig. 2. The antiproton energy spectrum at the top of the payload obtained in this work (Adriani et al., 2010b) compared with contemporary measurements: *Filled red circles:* Our results. *Asterisks:* (Aguilar et al., 2002). *Filled upward triangles:* (Abe et al., 2008). *Filled downward triangles, filled circles:* (Asaoka et al., 2002). *Open squares:* (Boezio et al., 2001). *Open upward triangles:* (Boezio et al., 1997). The curves show theoretical calculations for a pure secondary production of antiprotons during the propagation of cosmic rays in the Galaxy. (For interpretation of the references to colour in this figure legend, the reader is referred to the web version of this article.)

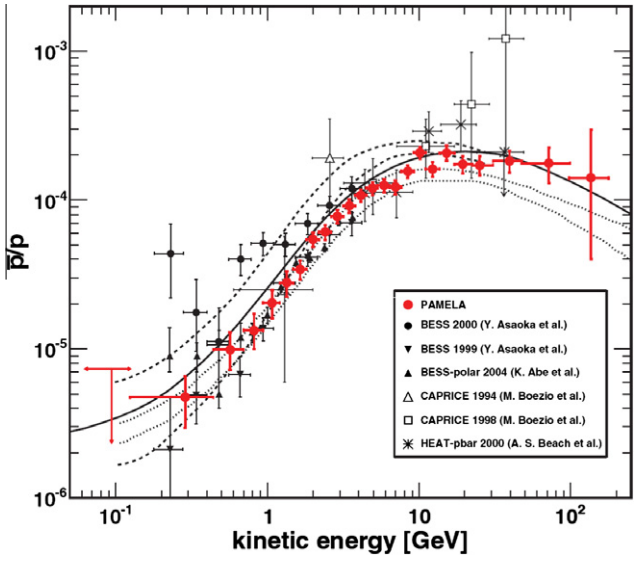

Fig. 3. The antiproton-to-proton flux ratio at the top of the payload obtained in this work (Adriani et al., 2010b) compared with contemporary measurements: *Filled red circles:* Our results. *Filled black circles, filled downward triangles:* (Asaoka et al., 2002). *Filled upward triangles:* (Abe et al., 2008). *Open upward triangles:* (Boezio et al., 1997). *Open squares:* (Boezio et al., 2001). *Asterisks:* (Beach et al., 2001). The curves show theoretical calculations for a pure secondary production of antiprotons during the propagation of cosmic rays in the Galaxy. (For interpretation of the references to colour in this figure legend, the reader is referred to the web version of this article.)

3.4. Antimatter (positrons)

The positron data need a very careful analysis because of the possibility of misidentification of protons as positrons: Since the proton-to-positron ratio increases from about 10^3 at 1 GeV to approximately 10^4 at 100 GeV, it is essential to have the rejection of the proton-background under control.

In the PAMELA analysis the particle identification was based on the combination of several observables: First the momentum measured by the tracker and the total energy measured in the calorimeter have to match. Further the starting point, the lateral and longitudinal profiles of the reconstructed shower had to fulfill specific selection criteria. Also the neutron detector response was taken into account.

This analysis technique has been tested at the proton and electron beams at CERN for different energies, by Monte Carlo simulations and by using flight data. We could prove that the proton contamination, measured at high energy (>10 GeV), was better than 10^{-5} on beam test data.

A different approach consists of keeping a very high selection efficiency and in quantifying the residual proton contamination by the mean of a so-called "spectral analysis" (Adriani et al., 2009).

By using the flight calorimeter data without any dependence on simulations or test beam data, we could obtain the proton distributions needed to estimate the contam ination.

Using this approach, the positron-to-all-electron ratio measured by the PAMELA experiment is given in Fig. 4, compared with other recent experimental results (see Adriani et al., 2009; Boezio et al., 2009).

In the same figure the GALPROP calculation (Moskalenko and Strong, 1998) for pure secondary production of positrons during the propagation of cosmic rays in the Galaxy without reacceleration processes is shown. As one can see, the positron fraction is expected to fall as a smooth function of increasing energy if secondary production dominates.

The data, covering the energy range 1.5–100 GeV, show two clear features. At low energies, below 5 GeV, the PAMELA results are systematically lower than data collected during the 1990s. This can be convincingly explained by effects of charge-dependent solar modulation: PAMELA positron/electron data have been collected during an A- phase when the positrons are modulated more than electrons, and this explains the difference at low energy with the results obtained by previous experiments that were performed in the A+ phase. The data from the AESOP experiment (Clem and Evenson, 2007), collected in the same A- phase as PAMELA, also support this statement.

At high energies, above 10 GeV, the PAMELA results show a positron fraction increasing significantly with energy. This excess of positrons in the range 10–100 GeV has led to many theoretical models explaining its origin

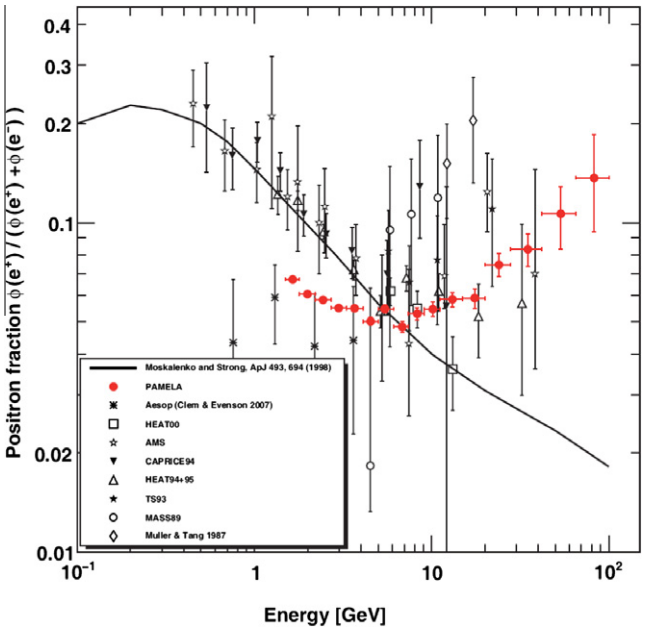

Fig. 4. The positron fraction measured by the PAMELA experiment (Adriani et al., 2009), compared with other recent experimental data: *Filled red circles:* Our results. *Asterisks:* (Clem and Evenson, 2007). *Open squares:* (Beatty et al., 2004). *Open stars:* (Aguilar et al., 2007). *Filled downward triangles:* (Boezio et al., 2000). *Open upward triangles:* (Barwick et al., 1997). *Filled stars:* (Golden et al., 1996). *Open circles:* (Golden et al., 1994). (For interpretation of the references to colour in this figure legend, the reader is referred to the web version of this article.)

as due to annihilation or decaying of dark matter. However, since the antiproton-proton ratio is compatible with a pure secondary production, there is some asymmetry between leptonic (positron fraction) and hadronic (antiproton-proton ratio) channels. This is difficult to explain in the framework in which a neutralino is the dominant dark matter component. The best explanations of the PAMELA data are obtained when assuming a direct leptonic annihilation channel for a wide range of the WIMP mass.

There are also astrophysical explanations such as nearby and young pulsars, objects well known as particle accelerators. Primary electrons are accelerated in the magnetosphere of pulsars in the polar cap and in the outer gap along the magnetic field lines emitting gamma-rays by synchrotron radiation, gammas that in the presence of pulsar gigantic magnetic field can evolve into positron and electron pairs. These, escaping into the interstellar medium, give a further contribution to the electron and positron components. See (Boezio et al., 2009) for a review.

Results published in Adriani et al. (2009) refer to data collected by PAMELA between July 2006 and February 2008. We analyzed a larger data set, collected between July 2006 and December 2008, and we applied a different statistical methodology (Adriani et al., 2010a). Fig. 5 shows the positron fraction obtained through a beta-fit with statistical and systematic errors summed in quadrature, compared with the PAMELA positron fraction of Fig. 4. The new experimental results are in agreement with what was

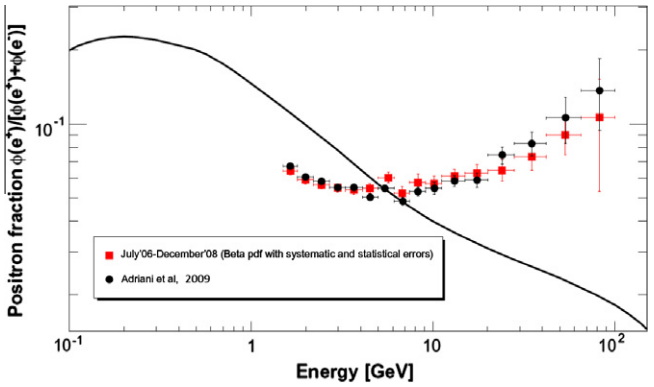

Fig. 5. The positron fraction obtained using a beta-fit with statistical and systematic errors summed in quadrature (red) (Adriani et al., 2010a), compared with the positron fraction reported in Fig. 4. (For interpretation of the references to colour in this figure legend, the reader is referred to the web version of this article.)

reported in Adriani et al. (2009) and confirm both solar modulation effects on cosmic rays with low rigidities and an anomalous positron abundance above 10 GeV.

An analysis of the PAMELA positron energy spectrum (up to ~300 GeV) will be presented in a future publication.

3.5. Antimatter (Antihelium)

The discovery of one nucleus of antimatter ($Z \geqslant 2$) in the cosmic rays would have profound implications for both particle physics and astrophysics. If there was primordial antimatter, antihelium would be the most likely form to be detected in cosmic rays, in the same way that in matter primordial nucleosynthesis results in helium being the most abundant element next to hydrogen. Several balloon-borne experiments searched for antihelium (WiZard, HEAT and BESS collaborations), and in 1998 the AMS-01 experiment installed on board of the space shuttle obtained cosmic ray data. The current lowest limit for the antihelium-to-helium ratio is of the order of 3×10^{-7} obtained by combining all of the BESS flight data (Sasaki et al., 2008). The PAMELA instrument will search for antihelium in an unprecented large energy range from a few hundred MeV to 600 GeV with a level of better than 10^{-6}. The analysis is in progress and the results should be published soon.

3.6. Electrons

Cosmic-ray electrons provide valuable information regarding the origin and propagation of cosmic rays in the Galaxy. Due to their low mass and the interstellar magnetic field, cosmic-ray electrons undergo severe energy losses during their propagation in the Galaxy, different from the cosmic-ray nuclear components at the same energy.

The PAMELA instrument is capable of doing a precision measurement of the electron component in the cosmic radiation, using similar seletion methods as presented above for the positron analysis. (Though the term "electron" is often used in the literature for total electrons (e+ plus e−), in this paper "electron" means explicitly "e−"). One can relax the selection criteria since the main background are only the rare antiprotons, and, mostly below 1 GV/c, locally produced pions. Only for high rigidities does the spillover contribution of protons become important. By requiring an electromagnetic-like interaction pattern in the calorimeter, all these contamination components were reduced to a negligible amount.

Great care has been taken to understand the instrumental effects such as selection efficiencies and energy determination. As in the analysis of the antiproton fluxes, we derived the selection efficiencies from flight data, cross-checking the results with those obtained using simulations of the apparatus based both on the GEANT3 (Brun et al., 1994) and GEANT4 (Agostinelli et al., 2003) packages. The validity of the simulations was confirmed by comparisons with test-beam and flight data.

Finally we used the rigidity measured by the magnetic spectrometer and unfolded the resulting energy spectrum to the top of the payload using a Bayesian approach (D'Agostini, 1995). In this approach the non-negligible energy loss of the electrons (primarily due to bremsstrahlung while traversing the pressurised container and parts of the apparatus prior the tracking system) was taken into account.

Since the PAMELA calorimeter is able to detect the total energy deposited by electromagnetic showers with a high precision, we could cross-check the results derived using the rigidity measured by the magnetic spectrometer with an independent measurement: The calorimeter energy resolution is Gaussian and varies from ≃8% at 10 GeV to ≃3% above 100 GeV, which is systematically different from the rigidity measurement. Thus the calorimeter provides a cross-check for the procedure used to unfold the electron rigidity spectrum to the top of the payload. Fig. 6 shows the electron energy spectra obtained using the calorimeter and the tracking information. We used the sign of the curvature in the magnetic spectrometer to select negative particles also for the calorimeter case, thus making a consistent comparison possible. The two sets of measurements are in good agreement. The observed 2% difference is fully accounted for by the uncertainty of the reconstruction and unfolding procedures.

Fig. 7 shows the electron energy spectrum measured by PAMELA along with other recent experimental data (see Adriani et al., 2011b). Note that the blue data points refer to measurements of the negative electron flux, measured by magnetic spectrometers like PAMELA, while data points with black symbols refer to the sum of electron and positron fluxes. Considering an additional positron component in these measurements of order a few percent, as was reported above, the agreement between PAMELA and the recent ATIC (Chang et al., 2008) and FERMI (Ackermann et al., 2010) data is quite good, taking statistical and systematic uncertainties into account. The PAMELA electron

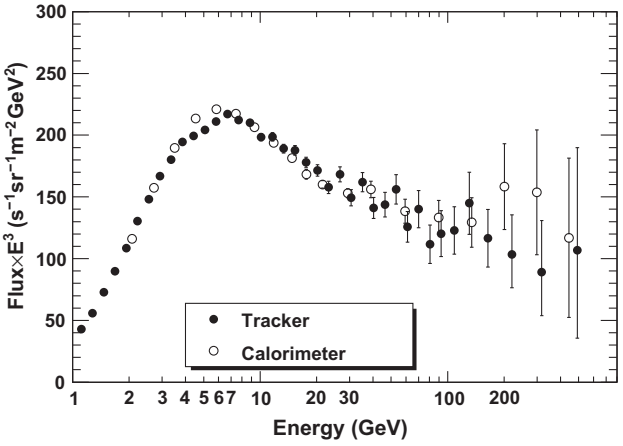

Fig. 6. The negatively-charged electron spectrum measured by PAMELA with two independent approaches: energy derived from the rigidity (full circles); energy derived from the calorimeter information (open circles). The calorimeter data refer to a smaller sample of particles due to stronger containment requirements to minimize the lateral leakage.

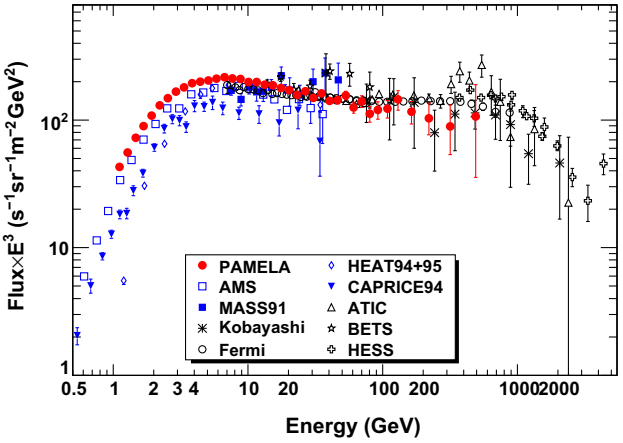

Fig. 7. The electron energy spectrum at the top of the payload obtained in this work (Adriani et al., 2011b) compared with some previous measurements. *Filled red circles:* Our results. *Open squares:* (Alcaraz et al., 2000). *Filled squares:* (Grimani et al., 2002). *Asterisks* (Kobayashi et al., 1999). *Open circles* (Ackermann et al., 2010). *Open diamonds:* (DuVernois et al., 2001). *Filled downward triangles:* (Boezio et al., 2000). *Open upward triangles:* (Chang et al., 2008). *Open stars:* (Torii et al., 2001). *Open crosses:* (Aharonian et al., 2008). The black symbols are used for instruments which measure the sum of electrons and positrons. (For interpretation of the references to colour in this figure legend, the reader is referred to the web version of this article.)

spectrum appears to be softer than those presented by ATIC and FERMI, which is consistent with a growing positron component with energy, but it is also compatible with the systematic uncertainties between the various measurements.

If one fits the electron data above 30 GeV (above the influence of solar modulation) with a single power-law, the spectral index is -3.18 ± 0.05.

Comparing our results with the commonly used GALPROP (Moskalenko and Strong, 1998) calculation, the agreement is quite good. However, our data can be better described by adding an additional primary electron component. We could also show that the PAMELA electron data can accommodate an additional component consistent with the positron fraction shown above.

Thus, the electron results are not inconsistent with the standard model of cosmic ray acceleration and propagation in the Galaxy. However, there is some disagreement between the data and the prediction that points to needed refinements of the propagation models and might require additional sources of cosmic rays. For more details see (Adriani et al., 2011b) and the discussion therein.

3.7. Proton and Helium Spectra

The most common particles in the cosmic radiation, protons and helium nuclei, are detected by PAMELA with very high statistics over a wide energy range, which allows to perform a precise measurement of their spectral shape. In the following we present the absolute cosmic ray proton and helium spectra in the rigidity interval between 1 GV and 1.2 TV. Data were gathered during the years 2006-2008.

The selection criteria could be chosen less strictly compared to the antimatter analysis, since now we just need to select the most abundant species. Proton and Helium candidates have been selected by using the energy loss in the tracker planes and the rigidity information. We defined selection criteria compatible with protons and He nuclei which removed positrons, pions and $Z \geqslant 2$. To separate the primary galactic component from the reentrant albedo component we used only particles above the local geomagnetic cutoff.

As in the antiproton analysis, the maximum detectable rigidity was evaluated for each event. Only events with estimated MDR greater than the measured rigidity were selected. As already discussed in the analysis of antiprotons and positrons, at high rigidities the finite spectrometer resolution can result in a wrongly assigned charge sign, or less dramatically, a wrong particle momentum, which finally will distort the measured spectra. Therefore the normalized rigidity distributions of selected protons and helium nuclei were corrected for the effects of rigidity displacement using the Bayesian approach of D'Agostini (1995).

Much work has been done to understand a possible global distortion of the spectrometer planes, which could mimic a track curvature, resulting in a shift of the measured deflection. This deflection systematic error was evaluated by studying the rigidity-over-energy ratio of electrons and positrons, whose energy can be measured with the calorimeter. In our case the estimated upper limit to the deflection systematic uncertainty due to tracking system alignment was $|\Delta d| < 10^{-4}$ GV^{-1}. This systematic effect has been accounted for as an additional uncertainty on the measured spectra and represents the dominant contribution to the total systematic error above $\simeq$200 GV.

Fig. 8 shows the proton and helium spectra measured by the PAMELA experiment compared to other recent experimental data. The fluxes are expressed in terms of kinetic

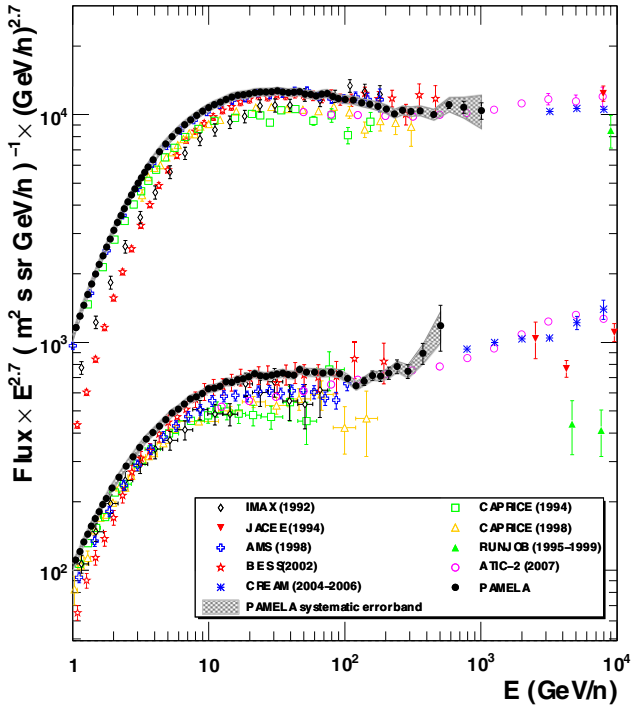

Fig. 8. Proton and helium absolute fluxes measured by PAMELA above 1 GeV/n, (Adriani et al., 2011a) compared with some previous measurements. *Filled black circles:* Our results. *Open diamonds:* (Menn et al., 2000). *Filled downward triangles:* (Asakimori et al., 1998). *Open crosses:* (Alcaraz et al., 2000). *Open stars:* (Haino et al., 2004). *Asterisks:* (Ahn et al., 2010). *Open squares:* (Boezio et al., 1999). *Open upward triangles:* (Boezio et al., 2003). *Filled upward triangles:* (Hareyama, 2006). *Open circles:* (Wefel et al., 2007).

energy per nucleon, converted from the rigidity measured in the tracker. For the conversion we assume pure proton and ^{4}He samples, therefore we will use the term 'proton' as a synonym for the more correct 'hydrogen'. Considering the statistical and systematic uncertainties of the various experiments, the results are in relatively good agreement. At low (<30 GeV) energies we expect differences due to solar modulation effects (our data were taken during a period of minimum solar activity). Previous data up to a few hundred GeV/n were collected by magnetic spectrometer experiments while higher energy data come from calorimetric measurements. Results from these instruments already inferred that proton and helium have different spectral indices at high energy or that a spectral deformation should occur at about 200 GeV, however, the statistical and systematic significance of those results were quite low compared to the PAMELA data (see Adriani et al. (2011a) and references therein).

The high energy (above 200 GeV/n) fluxes show a deviation from the power law: this is evident in Fig. 9, where the spectra of protons and Helium are shown as a function of rigidity. A change in the spectral index around 200 GV is visible for both spectra. To verify and quantify the presence of this change and the rigidity where this is occurring we applied the Fisher Student-t test. The test shows that for protons the single power law hypothesis is rejected at the 99.7% C.L. if we consider only statistical errors, or statistical errors combined with a positive systematic. In case of statistical errors with negative systematic the single power law hypothesis is rejected at the 95% C.L. The turnover in the spectrum occurs at 232^{+55}_{-30} GV with the spectral index changing from $\gamma_{80-232\mathrm{GV},p} = 2.85 \pm 0.015 \pm 0.004$ to $\gamma_{>232\mathrm{GV},p} = 2.67 \pm 0.03 \pm 0.005$.

For the helium data, the single power law hypothesis is rejected at the 95% C.L. with spectral hardening setting in at 243^{+27}_{-31} GV and a corresponding change of spectral index of $\gamma_{80-243\mathrm{GV}}$, $\mathrm{He} = 2.766 \pm 0.01 \pm 0.027$ to $\gamma_{>243\mathrm{GV}}$, $\mathrm{He} = 2.477 \pm 0.06 \pm 0.03$.

Another way to prove that p and He have different spectral indices is to plot the flux ratio as a function of the rigidity (see Fig. 10). The particle ratio has the advantage of reducing the systematic uncertainty due to geometrical factor, etc. In a magnetic spectrometer there is the additional advantage of cancelling the error associated with the alignment of the tracker and the track reconstruction algorithm. Fitting the spectral index of the ratio allows to measure the difference of the spectral indexes with a reduced systematic error. The value of $\Delta\gamma = \gamma_{He} - \gamma_p = 0.101 \pm 0.0014$(stat) ± 0.0001(sys) is in agreement with the aforementioned spectral indices. The ratio of p/He allows also to measure the value of $\Delta\gamma$ of the interstellar spectrum at regions below solar modulation. From the plot in Fig. 10 it is possible to notice that the ratio p/He is described by a power law fit down to rigidities as low as 5 GV.

These results challenge the standard theory that all nuclear species experience the same acceleration process at SNR and the same propagation processes in the Galaxy (see GALPROP Strong and Moskalenko, 1998 prediction, green[1], in Fig. 10).

One possible explanation is that populations of sources besides SNR could produce differences in the spectral characteristics for protons and helium. Also different populations of cosmic ray sources may explain the change in the spectra: one type of source, which may be of local origin, could efficiently accelerate cosmic rays up to hundreds of GeV and above this the spectrum is dominated by other sources such as SNR.

3.8. Primaries and secondaries

"Primary" nuclei are produced by stellar nucleosynthesis, while the "secondaries" are produced by fragmentation of primaries interacting with the matter of the interstellar medium. Thus the ratio of secondaries to primaries is directly related to the encountered amount of matter and to the nuclei lifetime before escaping from the Galaxy.

Measurements of the primary protons and helium were presented above, but PAMELA is also measuring carbon and oxygen nuclei, together with ^{3}He, lithium, beryllium

[1] For interpretation of color in Fig. 10, the reader is referred to the web version of this article.

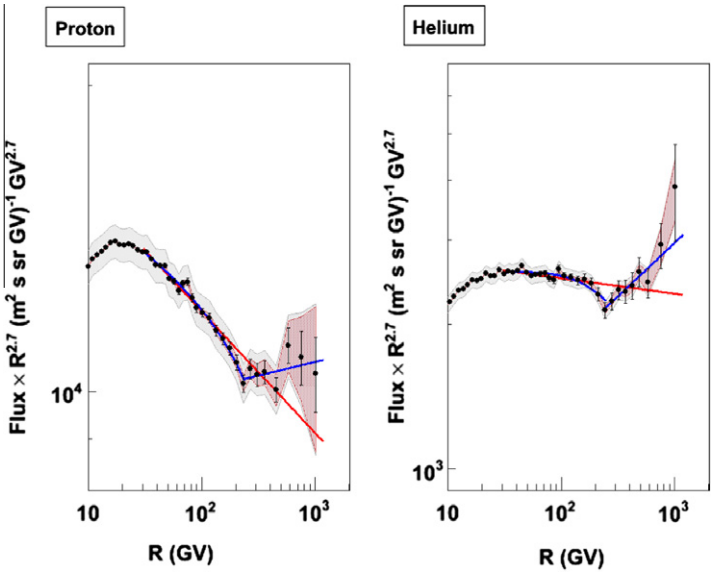

Fig. 9. Proton (left panel) and helium (right panel) spectra in the range 10 GV to 1.2 TV. The grey shaded area represents the estimated systematic uncertainty, the brown shaded area represents the contribution due to tracker alignment. The straight (red) lines represent fits with a single power law in the rigidity range 30 GV–240 GV. The blue curves represent the fit with a rigidity dependent power law (30–240 GV) and with a single power law above 240 GV. (Adriani et al., 2011a). (For interpretation of the references to colour in this figure legend, the reader is referred to the web version of this article.)

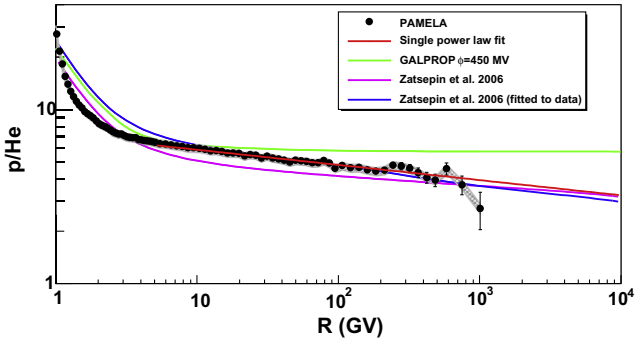

Fig. 10. Ratio of the flux between proton and helium data of PAMELA vs. Rigidity. The shaded area represents the estimated systematic uncertainty. Lines show different fits to the data (Adriani et al., 2011a).

and boron (secondaries). These data will constrain existing production and propagation models, providing detailed information on the galactic structure and the various mechanisms involved. The B/C ratio measured by PAMELA will be published very soon.

4. Conclusion

PAMELA is a general-purpose charged particle detector system exploring the antiparticle components of the cosmic radiation over a wide energy range. It has been in orbit since June 2006 and it is transmitting to ground 16 GB of data daily.

The main results obtained by PAMELA in 2009 concern the antiproton-to-proton and the positron-to-electron ratios, while recently the energy spectra of protons and alphas were published, and results for electron spectra and light nuclei are in preparation. These results are a big step forward to establish and understand scenarios of production and propagation of cosmic rays.

References

Abe, K., Fuke, H., Haino, S., et al. Measurement of the cosmic-ray low-energy antiproton spectrum with the first BESS-Polar Antarctic flight. Phys. Lett. B 670, 103–108, 2008.

Ackermann, M., Ajello, M., Atwood, W.B., et al. Fermi LAT observations of cosmic-ray electrons from 7 GeV to 1 TeV. Phys. Rev. D 82, 092004, 2010.

Adriani, O., Barbarino, G.C., Bazilevskaya, G.A., et al. An anomalous positron abundance in cosmic rays with energies 15–100 GeV. Nature 458, 607–609, 2009.

Adriani, O., Barbarino, G.C., Bazilevskaya, G.A., et al. A statistical procedure for the identification of positrons in the PAMELA experiment. Astropart. Phys. 34, 1–11, 2010a.

Adriani, O., Barbarino, G.C., Bazilevskaya, G.A., et al. PAMELA results on the cosmic-ray antiproton flux from 60 MeV to 180 GeV in kinetic energy. Phys. Rev. Lett. 105, 121101, 2010b.

Adriani, O., Barbarino, G.C., Bazilevskaya, G.A. et al. PAMELA measurements of cosmic-ray proton and helium spectra. Science. doi:10.1126/science.1199172, 2011a.

Adriani, O., Barbarino, G.C., Bazilevskaya, G.A., et al. The cosmic-ray electron flux measured by the PAMELA experiment between 1 and 625 GeV. Phys. Rev. Lett. 106, 201101, 2011b.

Agostinelli, S., Allison, J., Amako, K., et al. GEANT4-a simulation toolkit. Nucl. Instrum. Methods A 506, 250–303, 2003.

Aguilar, M., Alcaraz, J., Allaby, J., et al. The alpha magnetic spectrometer (AMS) on the international space station: part I-results from the test flight on the space shuttle. Phys. Rep. 366, 331–405, 2002.

Aguilar, M., Alcaraz, J., Allaby, J., et al. Cosmic-ray positron fraction measurement from 1 to 30 GeV with AMS-01. Phys. Lett. B 646, 145–154, 2007.

Aharonian, F., Akhperjanian, A.G., Barres de Almeida, U., et al. Energy spectrum of cosmic-ray electrons at TeV energies. Phys. Rev. Lett. 101, 261104, 2008.

Ahn, H.S., Allison, P., Bagliesi, M.G., et al. Discrepant hardening of cosmic-ray elemental spectra. ApJL 714, L89–L93, 2010.

Alcaraz, J., Alpat, B., Ambrosi, G., et al. Leptons in near earth orbit. Phys. Lett. B 484, 10–22, 2000.

Alcaraz, J., Alpat, B., Ambrosi, G., et al. Cosmic protons. Phys. Lett. B 490, 27–35, 2000.

Asakimori, K., Burnett, T.H., Cherry, M.L., et al. Cosmic-ray proton and helium spectra: results from the JACEE experiment. Astrophys. J. 502, 278–283, 1998.

Asaoka, Y., Shikaze, X., Abe, K., et al. Measurements of cosmic-ray low-energy antiproton and proton spectra in a transient period of solar field reversal. Phys. Rev. Lett. 88, 051101, 2002.

Barwick, S.W., Beatty, J.J., Bhattacharyya, A., et al. Measurements of the cosmic-ray positron fraction from 1 to 50 GeV. Astrophys. J. 482, L191–L194, 1997.

Beach, A.S., Beatty, J.J., Bhattacharyya, A., et al. Measurement of the cosmic-ray antiproton-to-proton abundance ratio between 4 and 50 GeV. Phys. Rev. Lett. 87, 271101, 2001.

Beatty, J.J., Bhattacharyya, A., Bower, C., et al. New measurement of the cosmic-ray positron fraction from 5 to 15 GeV. Phys. Rev. Lett. 93, 241102, 2004.

Boezio, M., Carlson, P., Francke, T., et al. The cosmic-ray antiproton flux between 0.62 and 3.19 GeV measured near solar minimum activity. Astrophys. J. 487, 415–423, 1997.

Boezio, M., Carlson, P., Francke, T., et al. The cosmic-ray proton and helium spectra between 0.4 and 200 GV. Astrophys. J. 518, 457–472, 1999.

Boezio, M., Carlson, P., Francke, T., et al. The cosmic-ray electron and positron spectra measured at 1 AU during solar minimum activity. Astrophys. J. 532, 653–669, 2000.

Boezio, M., Bonvicini, V., Schiavon, P., et al. The cosmic-ray antiproton flux between 3 and 49 GeV. Astrophys. J. 561, 787–799, 2001.

Boezio, M., Bonvicini, V., Schiavon, P., et al. The cosmic-ray proton and helium spectra measured with the CAPRICE98 balloon experiment. Astropart. Phys. 19, 583–604, 2003.

Boezio, M., Pearce, M., Picozza, P., et al. PAMELA and indirect dark matter searches. New J. Phys. 11, 105023, 2009.

Brun, R., Bruyant, F., Maire, M., et al. Detector description and simulation tool GEANT 3.21, DD/EE/94-1, CERN, Geneva, 1994.

Bruno, A. Cosmic ray antiprotons measured in the PAMELA experiment, Ph.D. thesis, University of Bari, <http://pamela.roma2.infn.it/>, 2008.

Chang, J., Adams, J.H., Ahn, H.S., et al. An excess of cosmic ray electrons at energies of 300–800 GeV. Nature 456, 362–365, 2008.

Clem, J., Evenson. Cosmic ray positron fraction observations during the a- magnetic solar minimum, in: Proc. 30th Int. Cosmic Ray Conf. (Merida), vol. 1, pp. 477–480, 2007.

D'Agostini, G. A Multidimensional unfolding method based on Bayes' theorem. Nucl. Instrum. Meth. A362, 487–498, 1995.

DuVernois, M.A., Barwick, S.W., Beatty, J.J., et al. Cosmic-ray electrons and positrons from 1 to 100 GeV: measurements with HEAT and their interpretation. Astrophys. J. 559, 296–303, 2001.

Golden, R.L., Grimani, C., Kimbell, B.L., et al. Observations of cosmic-ray electrons and positrons using an imaging calorimeter. Astrophys. J. 436, 769–775, 1994.

Golden, R.L., Stochaj, S.J., Stephens, S.A., et al. Measurement of the positron to electron ratio in the cosmic rays above 5 GeV. Astrophys. J. 457, L103–L106, 1996.

Grimani, C., Stephens, S.A., Cafagna, F.S., et al. Measurements of the absolute energy spectra of cosmic-ray positrons and electrons above 7 GeV. Astron. Astrophys. 392, 287–294, 2002.

Haino, S., Sanuki, T., Abe, K., et al. Measurements of primary and atmospheric cosmic-ray spectra with the BESS-TeV spectrometer. Phys. Lett. B 594, 35–46, 2004.

Hareyama, M. RUNJOB collaboration, high energy galactic cosmic rays observed by RUNJOB experiment. J. Phys. Conf. Ser. 31, 159–160, 2006.

Hofverberg, P. A New Measurement of Low Energy Antiprotons in the Cosmic Radiation, Ph.D. thesis, Royal Institute of Technology (KTH), Stockholm, <http://pamela.roma2.infn.it/>, 2008.

Kobayashi, T., Nishimura, J., Komori, Y. et al. High Energy Cosmic-Ray Electrons Beyond 100 GeV, in: Proc. 26th Int. Cosmic Ray Conf. (Salt Lake City), vol. 3, pp. 61–64, 1999.

Menn, W., Hof, M., Reimer, O., et al. The absolute flux of protons and helium at the top of the atmosphere using IMAX. Astrophys. J. 533, 281–297, 2000.

Moskalenko, I.V., Strong, A.W. Production and propagation of cosmic-ray positrons and electrons. Astrophys. J. 493, 694–707, 1998.

Picozza, P., Galper, A.M., Castellini, G., et al. PAMELA-A payload for antimatter matter exploration and light-nuclei astrophysics. Astropart. Phys. 27, 296–315, 2007.

Sasaki, M., Haino, S., Abe, K., et al. Search for antihelium: progress with BESS. Adv. Space. Res. 42 (3), 450–454, 2008.

Strong, A.W., Moskalenko, I.V. Propagation of cosmic-ray nucleons in the galaxy. Astrophys. J. 509, 212–228, 1998.

Torii, S., Tamura, T., Tateyama, N., et al. Energy spectrum of cosmic-ray electrons from 10 to 100 GeV observed with a highly granulated imaging calorimeter. Astrophys. J. 559, 973–984, 2001.

Wefel, J.P., Adams, J.H., Jr., Ahn, H.S. et al. Revised energy spectra for primary elements (H-Si) above 50 GeV from the ATIC-2 science flight, in: Proc. 30th Int. Cosmic Ray Conf. (Merida), vol. 2, pp. 31–34, 2007.